Automatic evaluation of stratum basale and dermal papillae using ultrahigh resolution optical coherence tomography

Jun Xie[a], Tian Hao[b], Xianghong Wang[a], Xiaojun Yu[c], Linbo Liu[a,*], Chengxin Li[b,*]

[a]*School of Electrical and Electronic Engineering, Nanyang Technological University, Singapore, 639798*
[b]*Chinese PLA General Hospital*
[c]*School of Automation, Northwestern Polytechnical University, Xi'an, Shaanxi, China, 710072*

Abstract

Diagnosis of many skin conditions requires evaluation of dermal papillae and stratum basale, such as vitiligo. In clinical practice, imaging dermal papillae structures relies on excisional biopsy followed by histological processing and analysis. As biopsy is invasive and associated with complications, a non-invasive imaging method such as optical coherence tomography (OCT) can complement the existing method by enabling large area scanning. However, because OCT imag analysis requires training and it takes time to review OCT images from large skin areas, an automatic evaluation method is preferred to reduce the workload and avoid 'sampling errors' during image analysis. Here we report an automatic method to enhance and detect dermal papillae and stratum basale in ultrahigh resolution OCT images. A high detection accuracy is achieved by rejecting image artifacts using a surface flattening algorithm and an artifact recognition algorithm. We further demonstrated the efficacy of this automatic method in detecting vitiligo in human subjects.

Keywords: Optical coherence tomography;dermal papillae, vitiligo

*Corresponding author

Email addresses: xiej0014@e.ntu.edu.sg (Jun Xie), 774093307@qq.com (Tian Hao), xh.wang@ntu.edu.sg (Xianghong Wang), XJYU@nwpu.edu.cn (Xiaojun Yu), LIULINBO@ntu.edu.sg (Linbo Liu), chengxinderm@163.com (Chengxin Li)

1. Introduction

As the deepest layer of the epidermis and the uppermost layer of dermis, stratum basale and dermal papillae stand for the boundary of dermis and epidermis. Stratum basale mostly consists of basal keratinocyte stem cells, which differentiated into other cells that forms the structures of epidermis. It also consists of other cells such as melanocytes, Langerhans cells and Merkel cells [1], which relates to skin pigment and immunity. Papillary dermis is composed of fine and loosely arranged collagen fibres as a supportive structure for the epidermis above. Dermal papillae are small extensions of the papillary dermis into the epidermis. They are in charge of exchange of oxygen, nutrients, and waste products between dermis and epidermis [2]. Therefore, the conditions of stratum basale and dermal papillae is closely related to many skin problems, such as aging, pigmented dermatosis (vitiligo, melasma, melanosis, etc.) and dermatoma (basal cell carcinoma, Paget's disease, melanoma, etc.).

To visualize and analyze the conditions of stratum basale and dermal papillae, current clinical optical diagnostic technologies includes histopathology and immunohistochemistry, Wood's lamp, dermatoscopy and confocal microscopy. Histopathology and immunohistochemistry require biopsy of skin, which could only sample a very small skin volume and associated with complications like trauma, scar, bleeding and pain. Though non-invasive, Wood's lamp and Dermatoscopy have been widely used in diagnosis of various skin conditions, their resolutions are not enough to observe dermal papillae structures. Confocal microscopy and optical coherence tomography (OCT) can provide better image resolution. In this study, we used OCT as our imaging method, and the pros and cons of confocal microscopy comparing with OCT will be further illustrated in section 4.3.

As a non-invasive medical imaging method, optical coherence tomography can provide cross-sectional and three-dimensional images of skin microstructures with a large scanning area (13 mm by 13 mm) and penetration depth of around 1-2 mm [3]. The spatial resolution of OCT may reach the cellular level [4], so that it allows identification of cellular structures based on the optical inhomogeneities [5]. However, although the applications of OCT in dermatology have shown promising results [6, 7], there have been few studies on the evaluation of dermal papillae and the stratum basale at high spatial resolutions (1-2 um) and validate the potential benefits of ultrahigh resolution OCT in the diagnosis of skin conditions.

This study aims at providing a non-invasive method to auto detect and analyze dermal papillae structures at a cellular level resolution using μOCT. As a non-invasive method, this study provides a possible solution for frequent monitoring and analysis of dermal papillae structures. And it could be helpful in diagnosis and early detection of numerous dermal papillae and stratum basale-related diseases, such as pigmented skin diseases like vitiligo.

2. Methodology

2.1. OCT system setup and data collection

We used a high-resolution OCT imaging system reported previously (Fig. 1) [7]. In brief, a broadband Supelum Broadlighters T-850-HP was used as light source (center wavelength $\lambda_c = 850\ nm$, bandwidth (FWHM) $\Delta\lambda_c = 165\ nm$, output power P=21.2mW). The incident light was split into the sample arm and reference arm by a 50:50 fiber coupler (TW850R5A2, Thorlabs Inc.) The sample light was colimated by a doublet (L1 and L3: AC080-015-B-ML, Thorlabs Inc.) before focused by an objective lens (L2 and L4: AC254-050-B-ML, Thorlabs Inc.) into the sample. The galvo scanner (GVSM002/M, Thorlabs Inc.) was used for transverse scanning of the subject. The reference arm was equiped with identical refractive optics as the sample arm to balance the dispersion.The backscattered light from the sample arm and the light reflected from the reference arm interfere at the fiber coupler, before half of it was received by the spectrometer. The spectrometer consists of a collimation lens (L5: AC127-030-B-ML, Thorlabs Inc), a diffraction grating (1200 1/mm@830nm, Wasatch Photonics Inc.), and a lined scanned camera (E2V AViiVA EM4) with a camera lens (Nikon AF Nikkor 85mm f/1.8D). The signal detected by camera was recorded by computer through an image acquisition card (KBN-PCE-CL4-F, Bitflow Inc.) at a resolution of 12 bits. The synchronization of the camera and galvo scanner was achieved through a computer-generated triggering signal.

The axial resolution and transverse resolution were measured to be 2.5um (in air) and 4.5 um, respectively. Cross-sectional images were acquired at an axial-line (A-line) rate of 30 kHz and 30 frames per second with 1024 A-lines per frame. It took 13 second to acquire a three-dimensional (3D) image containing 1024 $\times$ 1024 $\times$ 1024 voxels, which corresponds to 2.19 mm $\times$ 2.19 mm $\times$ 0.75 mm (Width x Height x Depth) in tissue.

We acquired 3D data from 10 normal human subjects and 2 patients with vitiligo. The study was approved by the Institutional Review Board at

Nanyang Technological University (IRB-2016-10-015). The writing consent was obtained from all subjects for each experiment. The measured sample power is around $2mW$, which conforms to the safety regulation of American National Standards Institute (ANSI) on maximum permissible exposure for skin.

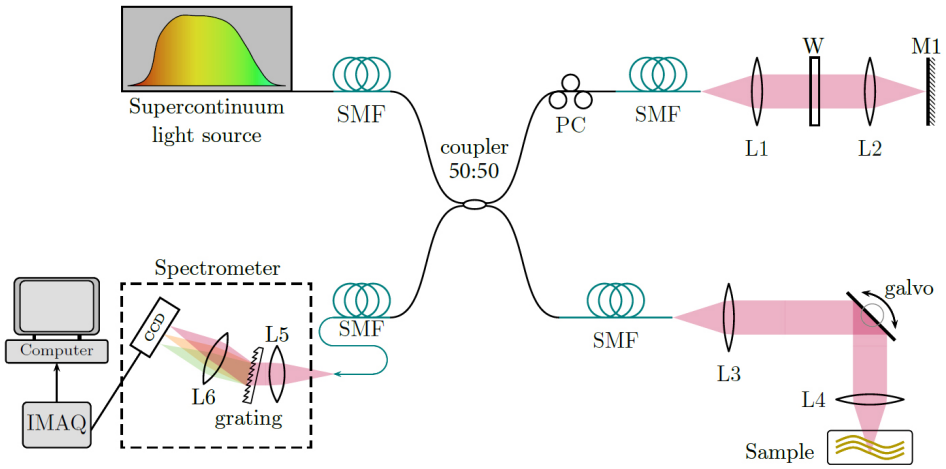

Figure 1: The schematic of the μOCT system setup. SMF: single mode fiber; L1 L5: achromatic lens; L6: camera lens; M1: mirror.

2.2. Overview of the automatic evaluation method

We have developed an automatic method that can enhance, detect, and analyze the dermal papillae based on their low scattering property with regard to the highly scattering property of the pigmented basal layer of the epidermis. Briefly, we firstly flattened the surface of the stratum corneum so that the depth variations of the stratum corneaum do not introduce errors into the dermal papillae detection; Secondly, we segmented the dermal papillae region based on the location of the second intensity peak of the average intensity along z-axis of the flattened OCT volume in the en face view; and lastly, we marked the dermal papillae regions for better visualization (Fig. 2). Each step of the procedure will be described in detail in the following sections.

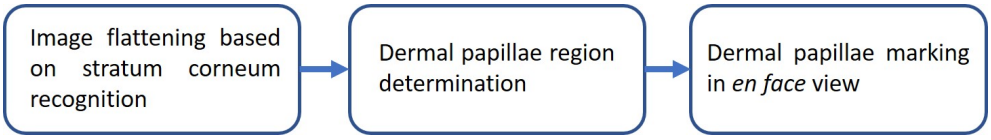

Figure 2: Basic flow chart of the image auto-analysis algorithm

2.2.1. Image flattening based on stratum corneum recognition

The depth location of the dermal papillae is affected by the irregular skin texture (Fig. 3(a).), which will make it difficult to realize the following segmentation and analysis of the image. Therefore, the first step of the algorithm is to detect the surface of the stratum corneum in the 3D OCT data and readjust each A-line along z-axis to flatten the surface of the stratum corneum.

Usually, a high-pass filter could provide boundary information in the depth direction. But the following detection errors may occur when setting the cut-off frequency: 1. If the cut-off frequency is low, the spatial accuracy will be sacrificed, and the information of structures within skin such as blood vessels will also be included; 2. If the cut-off frequency is high, it will be sensitive to the reflection signal of the glass window, the image signal-to-noise ratio, and image artifacts. In our auto-detect algorithm, two methods were used to solve this trade-off problem: detecting the region containing the surface of the stratum corneum followed by accurate determination.

Usually, a high-pass filter could provide boundary information in the depth direction. But the following detection errors may occur when setting the cut-off frequency: 1. If the cut-off frequency is low, the spatial accuracy will be sacrificed, and the information of structures within skin such as blood vessels will also be included; 2. If the cut-off frequency is high, it will be sensitive to the reflection signal of the glass window, the image signal-to-noise ratio, and image artifacts. In our auto-detect algorithm, two methods were used to solve this trade-off problem: detecting the region containing the surface of the stratum corneum followed by accurate determination.

1. Detecting the region containing the surface of the stratum corneum
   Studying the characteristic of OCT images of the stratum corneum, we observed that the surface of stratum corneum is in between the darker gel space and a brighter epidermis. As the determination of approximate region containing stratum corneum does not require high spatial resolution, to remove the high frequency noise , the OCT cross-

sectional images were median-filtered by a $(2r)^3$ kernel. r ranges from 10 to 20, within which the performances of the median filter and the following results do not change significantly.

$$I_M(x,y,z) = \frac{\sum_{i=x-r}^{x+r-1}\sum_{j=y-r}^{y+r-1}\sum_{k=z-r}^{z+r-1} I_o(i,j,k)}{(2r)^3} \tag{1}$$

where I_o is the original OCT image data, I_M is the median-filtered result.

The derivative of I_M along the depth direction clearly single out the region containing the surface of the stratum corneum and the glass window surface. (Fig. 3(b)):

$$I_D(x,y,z) = I_M(x,y,z) - I_M(x,y,z-1). \tag{2}$$

After the differentiation, we used an adaptive threshold to divide out the approximate region containing stratum corneum, considering the difference in average intensity of each A-line:

$$T_1(x,y) = k \cdot \max\left\{I_D(z)|_{x,y}\right\}. \tag{3}$$

where $T_1(x,y)$ is the threshold at transverse position (x,y), $\max\left\{I_D(z)|_{x,y}\right\}$ is the maximum value of $I_D(z)$ at (x,y). k is a scale factor. The value of k is inversely proportional to the depth range of possible stratum corneum region selected.

The approximate region containing surface of the stratum corneum was detected as I_w:

$$I_w(z)|_{x,y} = \begin{cases} 1 & I_D(z)|_{x,y} \geq T_1 x, y, \\ 0 & I_D(z)|_{x,y} \leq T_1 x, y, \end{cases} \tag{4}$$

To rule out the influence of glass window above stratum corneum and blood vessels beneath, a connected domain detection is applied on $I_w(z)|_{x,y}$ in the 3D dataset to find the largest connected domain of $I_w(z)|_{x,y}$. It can be seen that the detection covers all the stratum corneum surface, and successfully avoid interference from other surfaces such as glass window, stratum basale or blood vessels (Fig. 4(c)).

2. Detection of stratum corneum surface

Many human previous studies segmented skin images by detecting the intensity peak of the stratum corneum surface, assuming that it is the

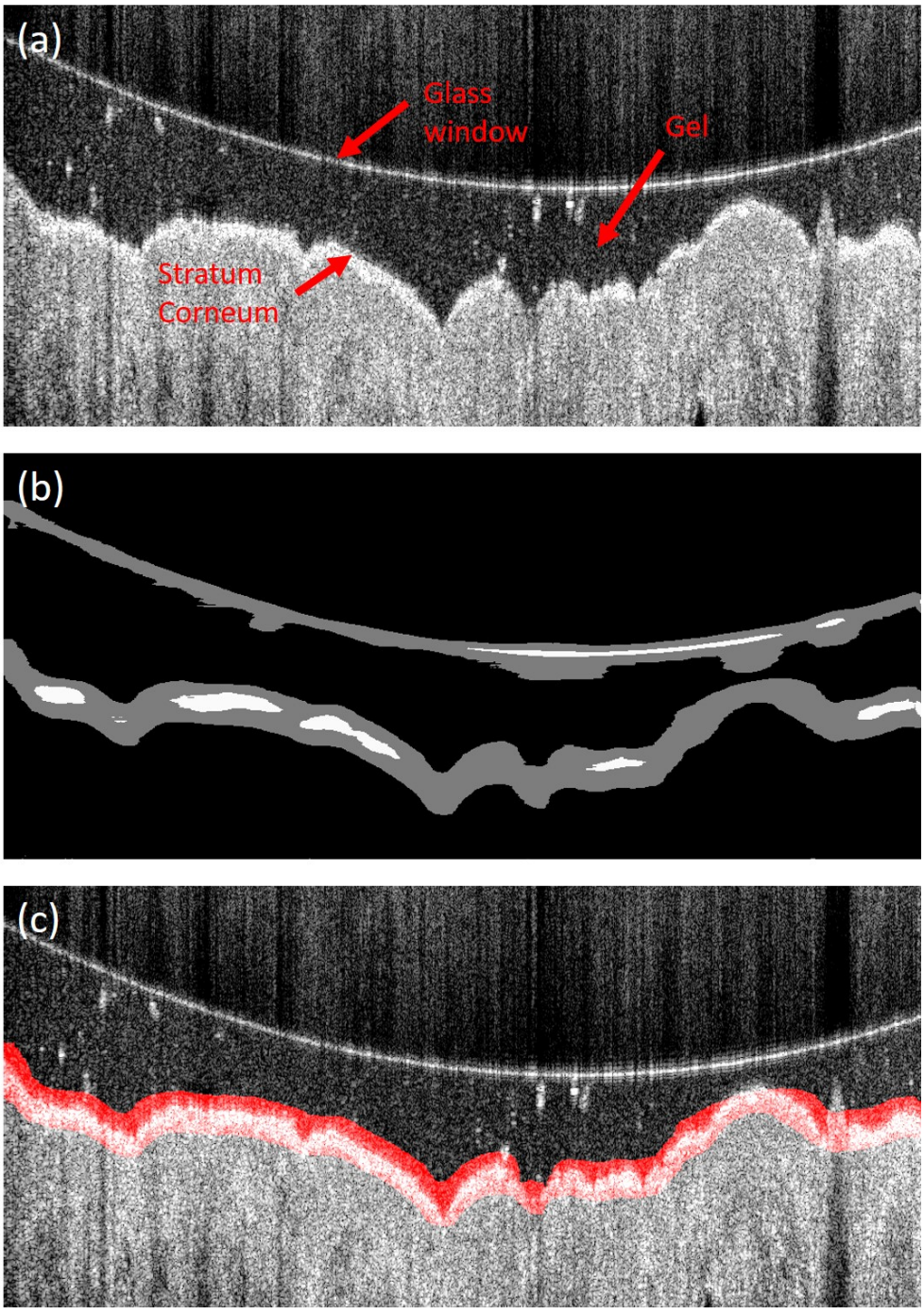

Figure 3: (a) A representative OCT cross-sectional image obtained from the forehead skin of a normal subject. (b) I_D: Differential result of the median-filtered I_o, with maximum value at around 3. (c) Possible stratum corneum region result marking on original OCT B-scan

highest along the z-axis. However, this assumption might not be true due to artifacts. In our study, instead of directly finding intensity peaks, a sinusoidal operator was applied to detect the intensity rising edge of the upper stratum corneum surface:

$$I_s(z)|_{x,y} = I_o(z)|_{x,y} * O_{sin}(i) \tag{5}$$

where $I_o(z)|_{x,y}$ is the original OCT image A-line at the-transverse position (x, y), and I_s is the result after the sinusoidal operator is applied (Fig. 4(b)). The sinusoidal operator is defined as:

$$O_{sin}(i) = \begin{cases} \sin(2\pi \frac{i-1}{L-1}), & i = 1, 2, \cdots, L; \\ 0 & otherwise. \end{cases} \tag{6}$$

where L is the length of the sinusoidal operator. In this case the value of L was set to be 10. We tested the value of L in the range of 5 to 20, and no significant influence on the result was found.

The sinusoidal operator can indicate the upper surface of the stratum corneum and the glass window (Fig. 4(b)). The result I_s is further median-filtered by a $10\times10\times10$ kernel to render a continuous boundary. I_w was used to reject the marginal information of glass window and stratum corneum in I_s,(Fig. 4(c)).:

$$I_R(x, y, z) = I_S(x, y, z)I_W(x, y, z). \tag{7}$$

The maximum point of each A-line in I_R was set as a start point matrix P_S:

$$P_S(x, y) = \max\left\{I_S(z)|_{x,y}\right\}. \tag{8}$$

In each A-line, search the intensity peak from the start point $P_S(x, y)$ for the location of the stratum corneum surface, which is shown in Fig. 4(d).

2.2.2. Dermal papillae region determination

All the A-lines of 3D OCT dataset were realigned so that the stratum corneum surface was at the same depth (Fig. 4e). The formation of the second peak (Fig. 5e, arrow) attributed to the highly scattering melanin granules within stratum basale, with which we can locate the depth range of the dermal papillae and evaluate the dermal papillae pattern in the *en face* view reconstructed from the 3D dataset.

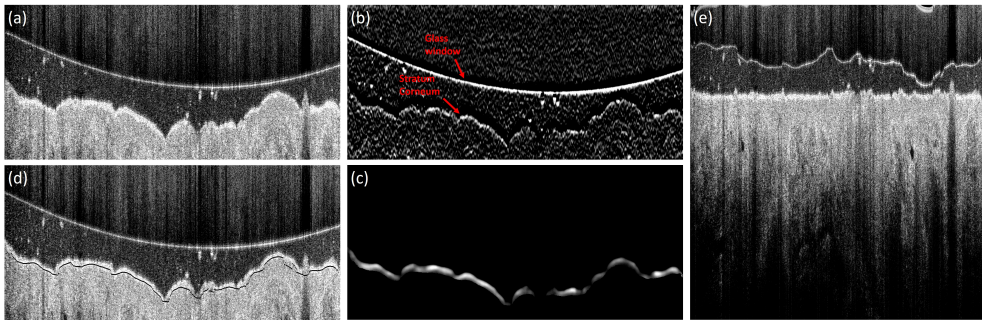

Figure 4: (a) Original OCT B-scan of human skin. (b) I_s: Result of applying the sinusoidal operator. (c) I_R: Truncated result of the median-filtered I_S. (d) Accurate location of the stratum corneum. (e) Realigned OCT B-scan based on stratum corneum location.

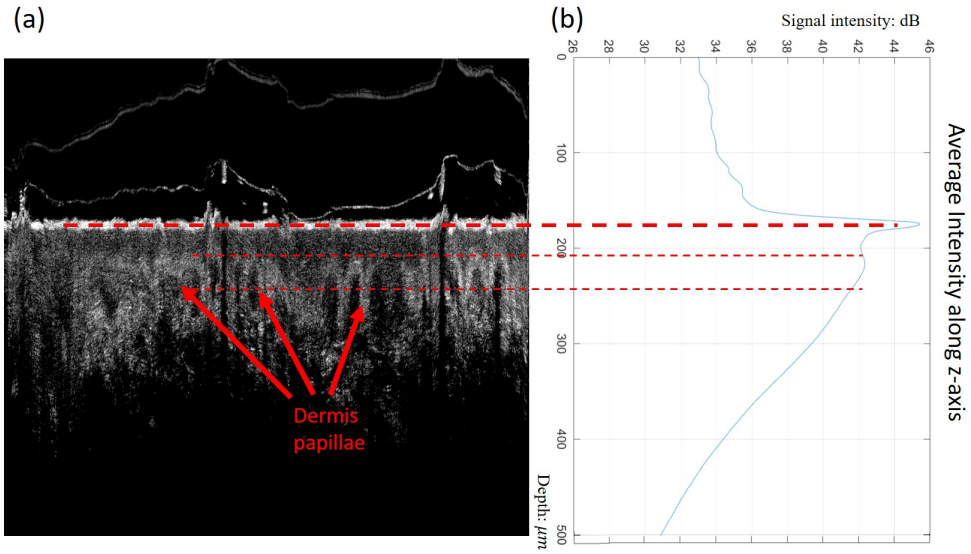

Figure 5: (a) Running average of 10 B-scan frames with adjusted brightness and contrast and (b) the corresponding average signal intensity along z-axis of the 3D OCT volume. The axis of the average signal intensity plotting corresponds to the depth of the OCT B-scan.

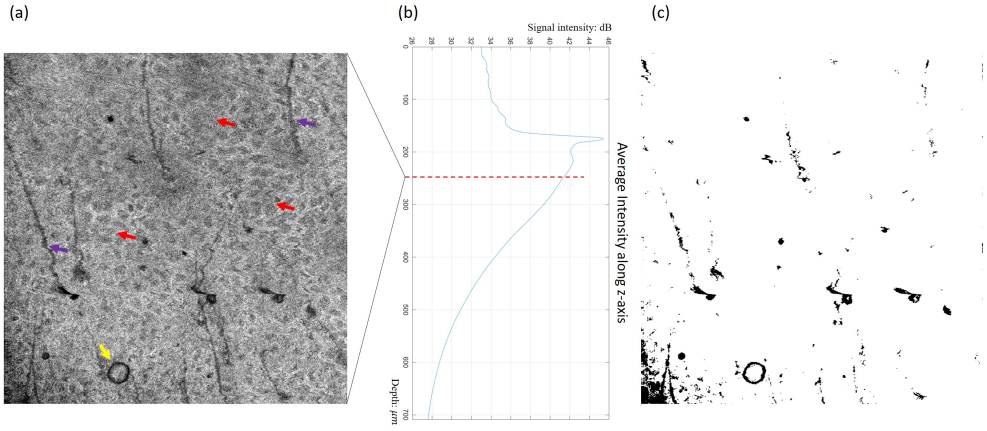

Figure 6: (a) *En face* view of dermal papillae layer and corresponding depth in (b) average A-line intensity plotting. Red arrow: porous patterns formed by intertwined dermal papillae structures and stratum basale of epidermis above. Purple arrow: artifacts of hairs. Yellow arrow: artifacts formed by waterdrops. (c) artifacts detection outcome.

2.2.3. Dermal papillae marking in the en face view

To reconstruct the *en face* view, we chose a depth location below the second peak, where the brighter part of the stratum basale above dermal papillae and the relatively darker part of dermis are intertwined together, resulting in obvious porous or spongy patterns in the *en face* view (Fig. 6).

1. Artifacts recognition
   Usually, image artifacts such as those caused by water droplets, hair and hair shafts significantly degrade the quality of the *en face* images [8] (Fig. 6) and should be removed before the marking of dermal papillae. Since these artifacts commonly create intensity shadows along the depth (Fig. 4 & 5, arrowheads), they can be singled out by their mean intensity over the whole depth range. To do so, an intensity range was set to distinguish the artifacts (Fig. 6c):

$$[M - 2S, M + 2S] \tag{9}$$

   in which M is the mean intensity value of the selected dermal papillae region, S is the standard deviation of mean values of each A-line.
2. Dermal papillae marking based on crosscorrelation pattern recognition
   To mark the dermal papillae structures in the en face view, we designed a model to simulate the intensity pattern of dermal papillae structures

(Fig. 7(a)). The model is a 31×31 pixel square, with a 15-pixel-radius low-intensity circle in the center and higher intensity periphery. The intensity at the second maximum peak of the average light intensity along z-axis (Fig. 5(b)) was used as the intensity of the periphery to represent the stratum basale. The average intensity at about 15 μm below the second intensity peak of dermal papillae was used as the intensity within the circle to represent the papillary dermis. The size of the circle was determined by the mean area of the transverse papillary dermis ($\sim 2 \times 10^4 \mu m^2$).

The dermal papillae were highlighted by cross-correlation between the simulation model and the *en face* image of the dermal papillae structures (Fig. 7(c)).

Subsequently, a threshold was set to isolate the dermal papillae structures from the background:

$$T = \mu + 2\sigma \tag{10}$$

In which μ and σ are the mean and standard deviation of the crosscorrelation result respectively. By removing the result within the nearby region of the previous recognized artifacts (Fig. 6(c)), the final determined dermal papillae structures are shown in Fig. 6(d).

3. Result analysis

3.1. Dermal papillae marking results

In the *en face* image shown in Fig. 7(d), we marked 452 dermal papillae structures. We compared the result produced by the automatic detection algorithm with that by manual selection in Fig. 7(e). The manual result was made by an experienced image analyst without prior knowledge of the auto-detection result. The specialist was asked to avoid the region of the previous detected artifacts (Fig. 6(c)). Due to the limitation of the image quality and manual labor, the specialist marked out only 226 structures. The manual recognized dermal papillae structures were marked by red dots.

Considering that the center of the manual labeled dots might not be exactly the same as the center of the auto-detection regions, the radius of the circle (15 pixels) in the dermal papillae simulation model (Fig. 7(a)) was used as deviation tolerance. If the center of the manual labeled dots deviates less than 15 pixels from the center of the corresponding auto-detection region, then this label is considered as successfully detected, and vice versa.

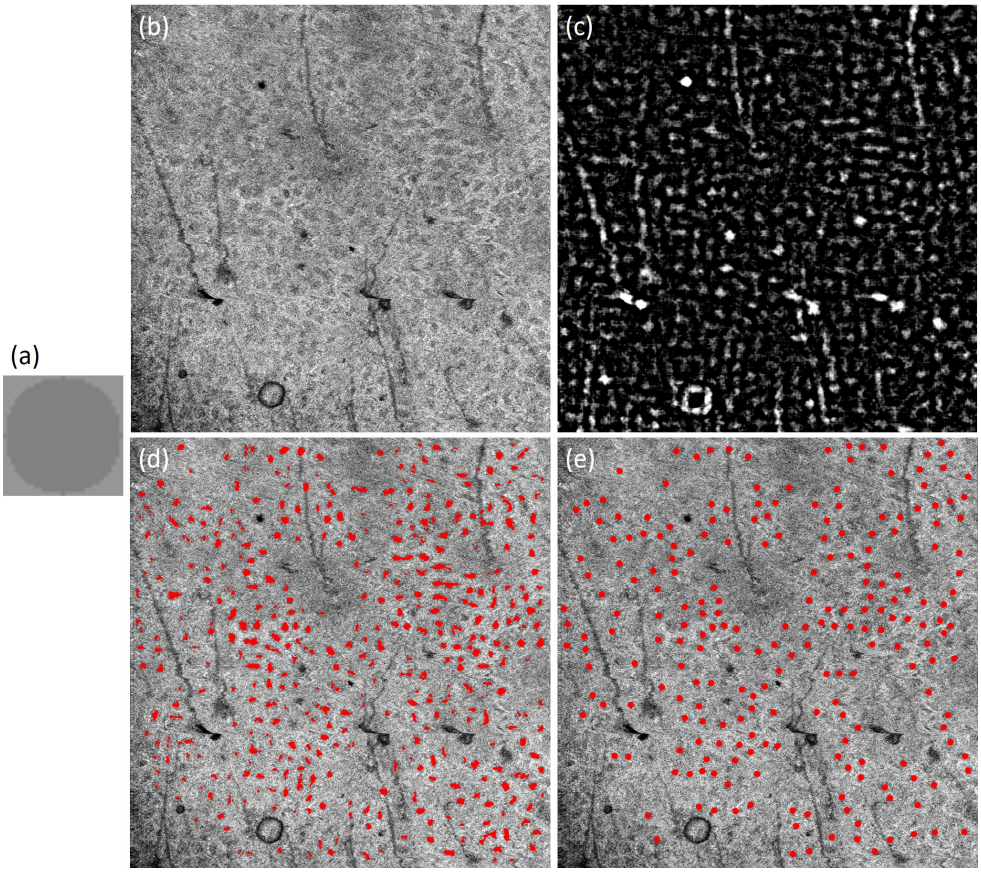

Figure 7: (a) Simulation model of the porous dermal papillae pattern. (b) *En face* view of dermal papillae layer. (c) The crosscorrelation result of the simulation model and the *en face* image of dermal papillae. The pixels with intensity lower than mean value is displayed as 0 in gray scale. (d) The "holes" of the porous dermal papillae structures is marked in red. (e) manual selected result.

The result shows that there are 209 manual labeled dots was successfully detected, resulting in a 92.92% detection rate. And by comparing the auto-detection result, more than 60% of the unpaired auto-detection region was further confirmed by the dermatology specialist. Due to the limitation of time and vigor, there are altogether 3 manual verified result of different subjects at different part of skins (subjects are adult males, scanning regions are opisthenar, forearm and forehead). The average detection rate is 91.71%.

3.2. Vitiligo detection

3.3. Vitiligo diagnosis

As the melanin granules within stratum basale are the major scatterers in the epidermis [9], our automatic dermal papillae detection method is sensitive to the anomalies of melanocyte-related diseases, such as vitiligo, melanosis and malignant melanoma. We studied OCT images acquired from an adult male patient with vitiligo lesions. The auto-detection method could detect little dermal papillae in images acquired from vitiligo lesions while abundant dermal papillae were detected in the normal control from the same patient (Fig. 8.).

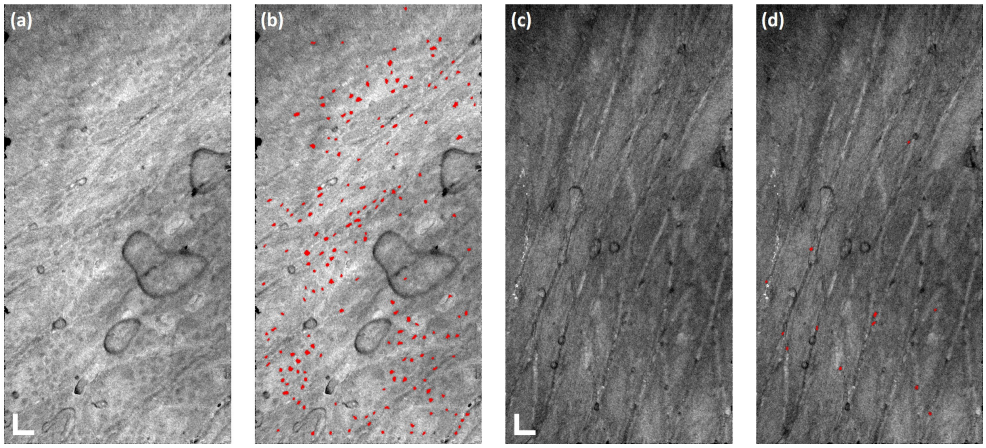

Figure 8: (a), (c): *en face* view of the dermal papillae region based on the realigned μOCT volume of normal skin (a) and vitiligo lesion (c). (b), (d): auto-detection result of dermal papillae structures of normal skin (b) and vitiligo lesion (d). Scale bar is equal to 100 μm.

In normal skin part, there are altogether 185 dermal papillae structures detected within 2.3762 mm^2 FOV. In lesion part, there are only 12 dermal papillae structures detected under the same FOV. The detected dermal

papillae density of normal skin and vitiligo lesion are 77.86 and 5.05 per mm^2 respectively.

4. Discussion

4.1. Vitiligo detection

Vitiligo patients suffer the loss or disfunction of the melanocytes which can no longer produce melanin. This should be reflected in OCT images as a decrease or absence of the above-mentioned scattering contrast between the stratum basale and dermal papillae. The result in Fig. 7 shows that the automatic evaluation method can be used in vitiligo diagnosis.

Though the symptoms of vitiligo are observable under naked eyes, this technology could still be very helpful in various aspects:

1. The dysfunction or damage of melanocytes in stratum basale will not be shown as skin lesions directly. It will take time for the melanin within epidermis to degrade before the skin-blotching conditions emerge. This technology could be useful in the early detection of vitiligo.
2. There are two phases of vitiligo: active phase and stable phase [10]. In active phase, the skin lesions will grow to other parts of healthy skin. It has been pointed out that melanocyte degeneration has been observed under non-lesion skins of possible vitiligo development [11]. This technology could be helpful in monitoring the changes of melanin distribution (granule or residue) during the active phase of vitiligo.
3. Sometimes the symptoms of decolorization by phenylphenol or other chemicals could be confounded with vitiligo. But this technology could give immediate answer as a non-invasive method.

4.2. Other stratum basale and dermal papillae related diseases

Apart from vitiligo, there are many other diseases which are closely related to the conditions of stratum basale and dermal papillae, such as melasma [12], melanosis [13], basal cell carcinoma [14] etc. This non-invasive imaging combined with automatic detection and analysis of dermal papillae could offer a three-dimensional histology-like information of conditions of dermal papillae and the stratum basale above.

Furthermore, this technology could also provide information of average thickness of different layers of skins. The part of algorithm in section 2.2.1. can provide us with information of average thickness of the stratum corneum,

the whole dermis layer as well as the dermal papillae. The anomalies of these thickness could auxiliary diagnose many skin lesions such as hyperkeratosis, parakeratosis/dyskeratosis, acanthosis, hypergranulosis, papillomatosis [2] etc. These lesions could be closely related to aging problems [15], lichen planus [16], squamous cell carcinoma [17], and acanthosis nigricans [18] etc. However due to the limitation of subjects, this project cannot provide imaging and detection results of these diseases. Further study is being carried on.

4.3. Comparison of confocal microscopy (CM) and OCT

There have been studies using confocal microscopy (CM) to study melanin related skin issues [9]. And CM does provide better spatial resolution ($\sim$ 1 μm) comparing with OCT (4.5 μm in this study). However, the field of view (FOV) in CM is not comparable with that of OCT, as OCT can adopt objective lens with smaller numerical aperture. Recent in vivo melanin related study using CM has a very limited FOV at around 0.5×0.5 μm, while the max FOV of our OCT imaging system is 8×8 μm. To acquire larger FOV, the usual method is to put together CM imaging results to form mosaics of CM images [19].

Furthermore, it has been mentioned that the section 2.2.1. of the importance and necessity of image flattening session if we are to do auto-detection and analysis of dermal papillae. And this image flattening can only be done with the three-dimensional image information provided by OCT.

4.4. Discussions of the auto-detection algorithm

Yasuno has done a skin detection work similar to the stratum corneum detection algorithm in this project [20]. There has been attempts using it to locate stratum corneum in our studies. However, this finding-maximum-peak algorithm always ends up locating the glass window instead of the stratum corneum below. Therefore, we were forced to develop this algorithm to better locate the stratum corneum under the presence of glass window before samples. The computation complexity is inevitably a bit higher comparing with Yasuno's, but it solves the problem of glass window perfectly. And the result of average intensity in depth after realigned μOCT volume (Fig. 6.) is very similar to that of Yasuno's, which verifies the accuracy of our algorithm.

The calculation of dermal papillae density in Sec.3.3 could be a bit lower due to the removal of artifacts in 2.2.3. Though it does not change the

dramatic difference between normal skin and lesion regions, a more accurate algorithm is being investigated to solve this problem.

Overall, the high-resolution OCT imaging system combined with the image auto-analysis algorithm can provide credible dermal papillae detection results in the en face view of the realigned OCT volume. As this non-invasive high-resolution detection and measurement of dermal papillae structures has no precedent, we used manual selection results to verify its accuracy. The above 90% detection rate is satisfactory.

This method could be very useful in early detection and auxiliary diagnose of several skin diseases such as vitiligo. We have tested this method on several vitiligo patients. The results indicate that this method is very sensitive to lesion and non-lesion part of skin. It has shown great potential of this method and its application in dermatology.

Acknowledgements

This research was supported in part by A*STAR Biomedical Research Council (H1701a008), National Natural Science Foundation of China (Grant No. 61705184), National Research Foundation Singapore (NRF-CRP13-2014-05), Ministry of Education Singapore (RG 83/18 (2018-T1-001-144)), NTU-AIT-MUV program in advanced biomedical imaging (NAM/15005), National Natural Science Foundation of China (81673043), and People's Liberation Army General Hospital fund (2016MBD-017).

References

[1] R. B. Weller, H. J. A. Hunter, M. W. Mann, Clinical Dermatology, FIFTH EDITION, 2015.

[2] Miller, J. Jeffrey, Lookingbill and Marks' principles of dermatology., Saunders Elsevier,, 2006.

[3] J. Mo, X. Yu, L. Liu, High Resolution Optical Coherence Tomography for Bio-Imaging, 2016.

[4] X. Yu, H. Tang, C. Hu, Q. Ding, L. Wang, X. Wang, Z. Fan, L. Liu, Multiscale skin imaging in vivo using optical coherence tomography, Laser Physics Letters 15 (7) (2018) 075601.

[5] J. Welzel, Optical coherence tomography in dermatology: a review, Skin Research & Technology 7 (1) (2010) 1–9.

[6] N. D. Gladkova, G. A. Petrova, N. K. Nikulin, S. G. Radenska-Lopovok, L. B. Snopova, Y. P. Chumakov, V. A. Nasonova, V. M. Gelikonov, G. V. Gelikonov, R. V. Kuranov, In vivo optical coherence tomography imaging of human skin: norm and pathology, Skin Research & Technology 6 (1) (2010) 6–16.

[7] A. Pagnoni, A. Knuettel, P. Welker, M. Rist, T. Stoudemayer, L. Kolbe, I. Sadiq, A. Kligman, Optical coherence tomography in dermatology, Skin Research and Technology 5 (2) (1999) 83–87.

[8] X. Yu, Q. Xiong, Y. Luo, N. Wang, L. Wang, H. L. Tey, L. Liu, Contrast enhanced subsurface fingerprint detection using high-speed optical coherence tomography, IEEE Photonics Technol. Lett. 29 (1) (2017) 70–73.

[9] M. Rajadhyaksha, M. Grossman, D. Esterowitz, R. H. Webb, R. R. Anderson, In vivo confocal scanning laser microscopy of human skin: melanin provides strong contrast, Journal of Investigative Dermatology 104 (6) (1995) 946–952.

[10] D. Ines, B. Sonia, B. M. Riadh, M. Slaheddine, T. Hamida, A. Hamadi, H. Basma, et al., A comparative study of oxidant–antioxidant status in stable and active vitiligo patients, Archives of dermatological research 298 (4) (2006) 147–152.

[11] A. Wańkowicz-Kalińska, R. M. van den Wijngaard, B. J. Tigges, W. Westerhof, G. S. Ogg, V. Cerundolo, W. J. Storkus, P. K. Das, Immunopolarization of cd4+ and cd8+ t cells to type-1–like is associated with melanocyte loss in human vitiligo, Laboratory investigation 83 (5) (2003) 683.

[12] N. P. Sanchez, M. A. Pathak, S. Sato, T. B. Fitzpatrick, J. L. Sanchez, M. C. Mihm Jr, Melasma: a clinical, light microscopic, ultrastructural, and immunofluorescence study, Journal of the American Academy of Dermatology 4 (6) (1981) 698–710.

[13] J. N. Kadonaga, I. J. Frieden, Neurocutaneous melanosis: definition and review of the literature, Journal of the American Academy of Dermatology 24 (5) (1991) 747–755.

[14] A. I. Rubin, E. H. Chen, D. Ratner, Basal-cell carcinoma, New England Journal of Medicine 353 (21) (2005) 2262–2269.

[15] Y.-H. Liao, W.-C. Kuo, S.-Y. Chou, C.-S. Tsai, G.-L. Lin, M.-R. Tsai, Y.-T. Shih, G.-G. Lee, C.-K. Sun, Quantitative analysis of intrinsic skin aging in dermal papillae by in vivo harmonic generation microscopy, Biomedical optics express 5 (9) (2014) 3266–3279.

[16] A. S. Boyd, K. H. Neldner, Lichen planus, Journal of the American Academy of Dermatology 25 (4) (1991) 593–619.

[17] C. J. Cockerell, Histopathology of incipient intraepidermal squamous cell carcinoma ("actinic keratosis"), Journal of the American Academy of Dermatology 42 (1) (2000) S11–S17.

[18] R. A. Schwartz, Acanthosis nigricans, Journal of the American Academy of dermatology 31 (1) (1994) 1–19.

[19] P. Guitera, S. Menzies, G. Argenziano, C. Longo, A. Losi, M. Drummond, R. Scolyer, G. Pellacani, Dermoscopy and in vivo confocal microscopy are complementary techniques for diagnosis of difficult amelanotic and light-coloured skin lesions, British Journal of Dermatology 175 (6) (2016) 1311–1319.

[20] Y. Hori, Y. Yasuno, S. Sakai, M. Matsumoto, T. Sugawara, V. D. Madjarova, M. Yamanari, S. Makita, T. Yasui, T. Araki, et al., Automatic characterization and segmentation of human skin using three-dimensional optical coherence tomography, optics express 14 (5) (2006) 1862–1877.